Chinese Chemical Letters 33 (2022) 3894–3898

Contents lists available at ScienceDirect

Chinese Chemical Letters

journal homepage: www.elsevier.com/locate/cclet

A composite PEO electrolyte with amide-based polymer matrix for suppressing lithium dendrite growth in all-solid-state lithium battery

Menghan Ge[a,1], Xiaoyu Zhou[a,1], Yinping Qin[a], Yang Liu[a,*], Jingjing Zhou[a], Xiaolei Wang[b,*], Bingkun Guo[a,*]

[a] Materials Genome Institute, Shanghai University, Shanghai 200444, China
[b] Department of Chemical and Materials Engineering, University of Alberta, Edmonton, Alberta T6G 2R3, Canada

ARTICLE INFO

Article history:
Received 29 June 2021
Revised 24 October 2021
Accepted 24 November 2021
Available online 29 November 2021

Keywords:
Composite
Amide
Lithium dendrite
Solid state electrolyte
Li metal battery

ABSTRACT

The lithium dendrite growth is still a serious challenge and impeding the realistic applications of all-solid-state lithium batteries. In view of the amide containing sediment layer can be stable on lithium/cathodes, a composite polymer electrolyte with amide-based matrix is *in-situ* built on porous electrodes. With the introduction of amide, the polymer electrolyte presents excellent ability to inhibit lithium dendrite growth and makes the Li/Li symmetric battery stably work for 500 h with a good ionic conductivity of 4.25×10^{-5} S/cm at 40 °C. The solid electrolyte also shows a wide electrochemical stable window and good interface contact with the porous cathode. Utilizing this composite polymer electrolyte, the all-solid-state Li/$LiFePO_4$ battery shows an initial discharge capacity of 146.5 mAh/g at 0.1 C under 40 °C and remains 81.4% in 100 cycles. The polymer electrolyte also can present better properties after modification. These results demonstrate that the presented PA-based composite polymer electrolyte could be served as a good electrolyte candidate for all-solid-state lithium-ion batteries.

The developing of electronic vehicles and large-scale energy storage devices calls for advanced lithium-ion batteries (LIBs) with high energy density and safety [1–3]. However, the state-of-the-art LIBs are still suffering the issues such as inflammability and unsatisfactory energy density [4,5]. The flaws are caused by the conventional liquid carbonate electrolytes with flammable property and narrow electrochemical windows which limit the choice of electrodes for LIBs [6,7]. Replacing the liquid electrolytes by solid electrolytes is an efficient method to address the drawbacks of commercial LIBs, since solid electrolytes are non-flammable and permit Li metal be utilized as the anode, which can significantly improve the safety and energy density of LIBs [8–11].

Inorganic ceramic electrolytes, such as $Li_7La_3Zr_2O_{12}$(LLZO), $Li_{1.3}Al_{0.3}Ti_{1.7}(PO_4)_3$(LATP), $Li_2S{-}P_2S_5$ and $Li_2S{-}SiS_2$ [12–19], have been investigated extensively because of their high mechanical strength and ion conductivities. Nonetheless, inorganic solid electrolytes' interfacial compatibility with porous electrodes and machining properties are still the serious challenges in industrial application and cannot satisfy the requirements of commercial LIBs [20–24]. By contrast, the solid polymer electrolytes (SPEs), such as poly(acrylonitrile), poly(propylene carbonate) and poly(ethylene carbonate) [25–29], are considered to be more suitable for the application of lithium-ion batteries due to their better interfacial properties on cathodes, superior flexibility and scalable [30–33]. Among the SPEs, polyethylene oxide (PEO)-based polymer electrolytes are regarded as the most promising candidates to prepare all-solid-state LIBs since 1970s due to the relatively low industrial cost, good film forming effect and excellent ability to complex with lithium salts [34–37].

However, PEO-based polymer electrolytes present poor interfacial strengths/stabilities at their operating temperature on lithium metal anode, which tends to cause the growth of Li dendrite and the failure of batteries in cycling [38]. To tackle the issue, tremendous efforts have been focused on ameliorating the interfacial properties of PEO SPEs. Introducing inorganic fillers with high modulus into SPEs is a widely adopted strategy. The ionic conductive or insulative particles, such as h-BN [39], LiF [40,41], Al_2O_3 [42], SiO_2 [43], LLZO [44], LATP [45–47], were utilized to enhance the mechanical property of PEO electrolytes for suppressing Li dendrite growth. However, the dispersing of particle fillers in PEO is a big challenge in SPE preparation technique [48]. Fabricating crosslinking polymer networks in PEO electrolytes is an-

* Corresponding authors.
E-mail addresses: liuyang81@shu.edu.cn (Y. Liu), xiaolei.wang@ualberta.ca (X. Wang), guobingkun@shu.edu.cn (B. Guo).
[1] These authors contributed equally to this work.

https://doi.org/10.1016/j.cclet.2021.11.073
1001-8417/

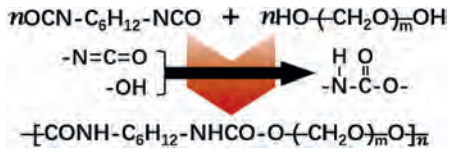

Scheme 1. The reaction mechanism between PEG and HDI.

other choice. Guo *et al.* proposed a PEO electrolyte with an interpenetrating poly(ether−acrylate) network [49]. This SPE presents really high mechanical strength ~12 GPa, and makes a Li/Li symmetric cell works at 4 mA/cm^2 for 130 h. Other polymers like polycarbonate [50], polystyrene [51], poly(acrylonitrile) [52], polyvinylidene fluoride [53], poly(*m*-phenylene isophthalamide) [54] also can exhibit the similar abilities. Nonetheless, most of the SPE design ideas focus on the Li anode interface only and lack the comprehensive consideration about electrochemical stability/interface compatibility of the SPEs on cathodes [55,56].

In the work we reported previously, introducing amide group into solid electrolyte interphase (SEI) on anode can make a smooth uniform surface on Li metal anode in cycling with the Young's modulus as high as 10 Gpa [57]. On the other side, carbonyl in amide group is a good electron donor, which would enhance the dissociation of lithium salts, increasing the density of the carrier in SPEs. Carbonyl also can interact with other electron acceptors, such as the methylene in PEO, by hydrogen bond, van der Waals force, or other weak interactions. This means the amide-containing compound would composite with PEO. Furthermore, amide group can be formed by isocyanate and hydroxyl *via* thermodynamic processes, and amide group is electrochemical and thermodynamics stable on both of Li metal and cathodes with high operating potential (>4.7 V *vs.* Li$^+$/Li) [58–60]. The former means amide compound can be *in-situ* formed on the cathodes which enhance the wettability of SPEs on porous electrodes, and the latter means the wider electrochemical stable window of amide-containing SPE than that of PEO. Thus we try to *in-situ* construct a composite polymer electrolyte (PPA) consisting of both PEO filler and an amide-based polymer matrix (PA) produced with 1,6-hexamethylene diisocyanate (HDI) and poly(ethylene glycol) (PEG) on cathode. The electrolyte membrane shows a wide electrochemical stability window up to 4.7 V *vs.* Li$^+$/Li, good compatibility with porous cathode, and considerable suppression capability of lithium dendrite growth as expected. In addition, the SPE also shows high ionic conductivity which should be attributed to the low crystalline phase of the polymer caused by the interaction between polymer matrix and PEO. Aforementioned advantages of this SPE make the Li/SPE/Li cell work more than 500 h and $LiFePO_4$/SPE/Li battery work stably under 40 °C.

The PPAs were produced as shown in Experimental section and Table S1 (Supporting information). Fourier transform infrared spectroscopy (FTIR) was utilized to investigate the polymerization between HDI & PEG and the interaction between the product and PEO (Fig. 1a). The absorption peaks at 2270 cm^{-1} and 1900 cm^{-1} disappear after the reaction, which are related to N=C=O of HDI and end OH in polyethylene oxide samples, and the new peaks at ~1537 and ~1680 cm^{-1} belonging to N–H and C=O are observed in the products, suggesting the successfully producing of amide group [61]. As shown in Scheme 1, the reaction mechanism should be a hydroxy reacts with an isocyanate would produce amide group. Considering the M_w of PEO is 300,000 g/mol and PEG is 200 g/mol, and the compound with smaller molecular presents higher reaction activity with HDI in polyethylene glycols, these data indicate the successfully polymerization between HDI and PEG, and no free monomer can be detected in PA and PPAs. In the polymerization products, the stretching vibration bands around

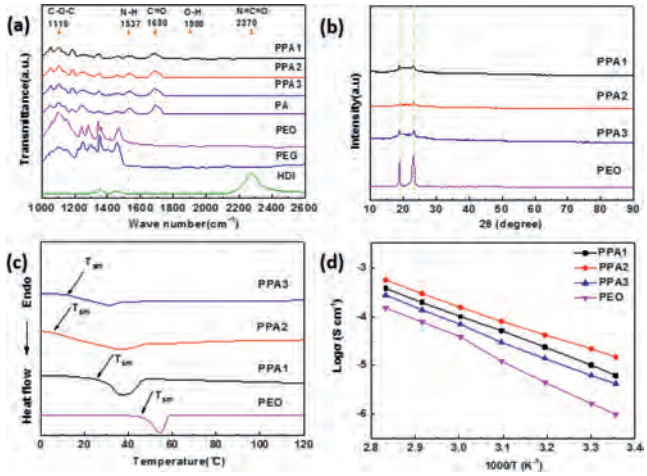

Fig. 1. (a) FTIR, (b) XRD patterns, (c) DSC curves and (d) ionic conductivities of the SPE films.

1110 cm^{-1} belonging to C–O–C of PEO show slight shifts in PPA samples, implying the interaction between the polymer matrix PA and PEO. A slight red shift trend is detected around 1680 cm^{-1} in PA and PPAs. Combined with the contents of PEO in PPAs, this should be understood as the formation of H-bond between CH_2(PEO) and carbonyl(PA), which lower the bond energy of carbonyl. Moreover, the C–O–C peak of PEG shows no obvious shift in PPAs should be the supplementary evidence for PEG precedes PEO reacts with HDI, and the decrease of the peak displacement from PPA1 to PPA3 suggests the fading of the interaction between PEO and PA in the composite electrolytes.

The interaction between PA and PEO may influence the performances of PPAs in different measurements. As shown in Fig. 1b, the PEO film shows two sharp peaks at 19.2° and 23.6° in X-ray diffraction (XRD) diagram, and the similar peaks of PPAs are much weaker and wider, meaning the lower crystallinity of EO segment (CH_2-CH_2-O) in PPAs [62]. PPA2 shows the weakest and widest peaks among the samples, meaning the lowest crystallinity in those of PPAs. The peaks of PPA1 and PPA3 is a little sharper. Combined with FTIR curves (Fig. 1a) and the composition of PPAs (Table S1 in Supporting information), these mean there are more segregation in PPA1 and PPA3, which should be carbonyl-EO and EO segment. Differential scanning calorimetry (DSC) test was carried out to investigate the start melting temperature (T_{sm}) of polymer electrolytes. As showed in Fig. 1c, an endothermic peak started at 45.2 °C in the curve of pure PEO electrolyte. With the adding of PEO, the T_{sm}s of PPAs decrease significantly and the peak areas gradually reduces. The results also should be related to the interaction between PA and PEO which suppresses the crystallization of PEO. Although PPA3 exhibits the lowest melting peak, PPA2 shows the lowest T_{sm} at 5.3 °C, suggesting this sample may present particular properties. Considering T_{sm} should be related to the crystallinity of polymer, and crystallinity affects the ionic conductivity of polymers, the DSC result is consistent with the XRD patterns (Fig. 1b) and suggests the good ionic conductivity of PPA2. Then the ionic conductivities of electrolytes were measured by electrochemical impedance spectrum (EIS) at various temperatures in the Fig. 1d. The ion conductivities of PPAs are higher than PEO at all of the temperature. These results should be related to the interaction between PA(carbonyl) and PEO(CH_2) and the interaction between carbonyl and Li$^+$. Comparing to those of PEO, the former reduces the activation energies (Table S2 in Supporting information), the crystallinities and the melting points of the composites, and the latter increases the density of the carrier in SPEs by enhancing the dissociation of lithium salts. The carbonyl in amide

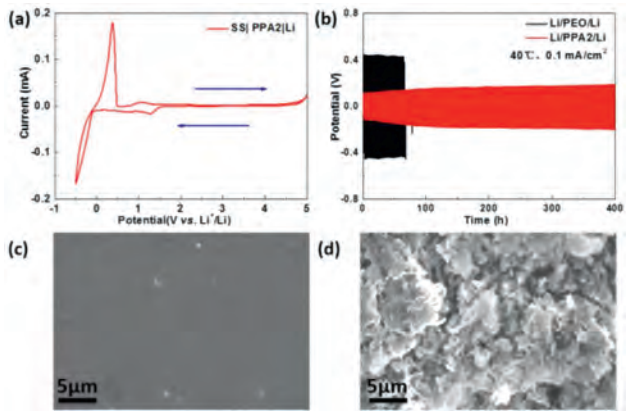

Fig. 2. (a) Cyclic voltammetry curve of Li/PPA2/SS battery at a scan rate of 0.1 mV/s from −0.5 V to 5 V at 40 °C. (b) The potential profiles of Li plating/striping in Li/PPA2/Li and Li/PEO/Li symmetric battery at 40 °C under a current density of 0.1 mA/cm^2. (c, d) SEM images of Li metal anodes from Li/PPA2/Li and Li/PEO/Li battery after cycling at 40 °C.

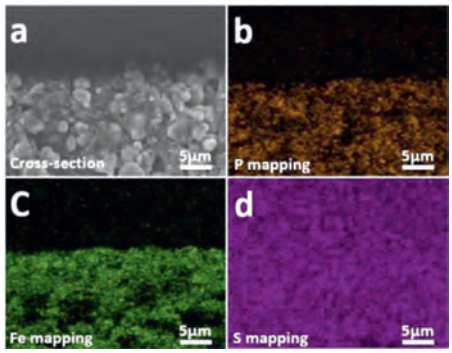

Fig. 3. (a) The cross-section of $LiFePO_4$/PPA2. (b) The P, (c) Fe, (d) S element distributions on the $LiFePO_4$/PPA2 cross section.

group may participate in the dissociation of lithium salts. Moreover, the composite electrolyte PPA2 shows the highest ion conductivity in all of the samples and 4.25 × 10^{-5} S/cm at 40 °C, matching the lowest activation energy, crystallinity and T_{sm} in those of PPAs. The lithium-ion transference number of the films was tested *via* the potentiostatic polarization method with the polarization of 10 mV, and the lithium-ion transference number of PEO and PPA2 were calculated to be 0.14 and 0.31 (Fig. S1 in Supporting information). This demonstrates the electrolyte design strategy can make the lithium-ion transference number of base SPE more than double, and the composited SPE system appear to be more favorable to the transportation of lithium-ions than that of anions, which should be attributed to the interaction between amide and PEO.

Considering amide group is electrochemical stable at high potential, the electrochemical window of PPAs should be expanded basing on PEO. Then linear sweep voltammetry (LSV) was carried out to investigate the electrochemical stabilities of the composite electrolytes in SS/PPAs/Li batteries at 40 °C (Fig. S2 in Supporting information). The PPAs show lower currents at high potential than that of PEO, which is oxidized >4 V *vs.* Li^+/Li in the works reported [63,64]. Furthermore, PPA2 presents the highest electrochemical stability, and be stable at the whole electrochemical window between 0 and 4.7 V *vs.* Li^+/Li in the cyclic voltammetry (CV) measurement as shown in Fig. 2a.

DMA measurement has been taken to investigate the effect of amide polymer on the films' mechanical properties. The stress-stain curves show the PPA2's fracture strength is >1 MPa and Young's modulus is ~34 MPa, meanwhile those of PEO are 0.28 and 10 MPa (Fig. S3 in Supporting information). Basing on the stress-stain curves, calculation displays the toughness of PPA2 is 2.8 times higher than that of PEO film, meeting the flexing test results (Fig. S4 in Supporting information). These also should be related the introduction of amide, which forms hydrogen bond reciprocity between carboxyl groups and methylene groups as shown in Fig. 1a, leading to the obvious improvement of the composited polymer's mechanical properties [57].

Then Li/SPE/Li cell was investigated in Fig. 2b under 0.1 mA/cm^2 at 40 °C. The cell utilizing PPA2 presents a relative low over-potential ~0.18 V in the cycling more than 500 h (250 cycles) without evident short circuiting, indicating the good electrochemical and thermodynamics stabilities between PPA2 and lithium metal. However, the Li/PEO/Li cell presents a much higher over-potential ~0.45 V and shorts in 70 h cycling (35 cycles). In the work reported [57], the introduction of amide would enhance the mechanical characteristic and conductivity of the polymer, which inhibit the Li dendrite growth dramatically. In this work, the composition of amide also presents similar characteristics. The lithium metal obtained from the Li/PPA2/Li cell after the test is smooth and dendrite-free (Fig. 2c), which is similar to that before cycling as shown in Fig. S5 (Supporting information). In contrast, the lithium metal obtained from $LiFePO_4$/PEO/Li battery is much rougher with mossy dendrites (Fig. 2d). The cross-sections also present the similar phenomenon (Fig. S6 in Supporting information). In Fig. 1d, Figs. S3 and S4, PPA2 presents good conductivity and mechanical characteristics. The former means the uniform electric field of the Li metal surface which increases the tendency of the uniform deposition of lithium metal, and the latter inhibits the growth of Li dendrites. Both of these make the smooth surface of Li anode in Li/PPA2/Li cell.

The surface and cross-section morphology of PPAs and $LiFePO_4$/PPA2 were examined by the scanning electron microscope (SEM) to study the compatibility between the composite electrolytes and cathode. The surface morphology of PPAs are smooth without obvious crack or components segregation as shown in Fig. S7 (Supporting information), suggesting the homogeneous phase distribution of the composite electrolytes' components. There is also no evident crack or gap between the solid electrolyte and $LiFePO_4$ cathode (Fig. 3a), meaning the good contact between PPA2 and the cathode. The mapping measurement was taken to investigate the element distribution in the SPE and cathode. Fe element and P element are detected in the similar location in Figs. 3b and c, and S element is relatively uniformly distributed in the full image of Fig. 3d. In view of $LiFePO_4$ is the only source of Fe and P element, and S element comes from LiTFSI in the solid electrolyte, the data presented above further confirm that the monomer mixture can penetrate into the porous cathode and evenly *in-situ* polymerized inside the $LiFePO_4$ cathode. Furthermore, there is a sharp boundary of the porous cathode in Fig. 3a which is similar to Figs. 3b and c, and no boundary can be detected in Fig. 3d. The frontier confirms the integrity of $LiFePO_4$ cathode while the SPE is *in-situ* built, and the latter suggests the close contact of SPE and the $LiFePO_4$ particles. The good interfacial contact and uniformly distribution of the polymer electrolyte on and inside the cathode will be favourable for reducing the interfacial impedance between PPA2 and $LiFePO_4$ electrode.

To investigate the electrochemical performance of PPA2 in all-solid-state batteries, $LiFePO_4$/PPA2/Li batteries were assembled. The electrochemical impedances of $LiFePO_4$/PPA2/Li batteries were tested by EIS at 40 °C (Fig. 4a). The interface impedance of *in-situ* prepared $LiFePO_4$/PPA2/Li battery is much lower than that of the *ex-situ* prepared one, confirming the favourable interfacial compatibility between PPA2 and $LiFePO_4$ cathode prepared by *in-situ* method as we expected. The charge/discharge performance of the

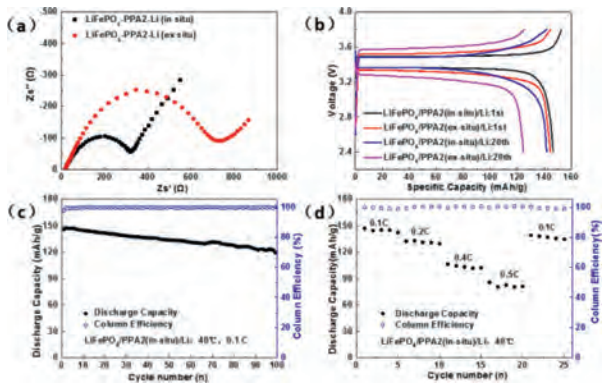

Fig. 4. (a) The electrochemical impedance spectroscopy, (b) the charge/discharge curves, (c) the long cycling performance and (d) C-rate cycling performance of $LiFePO_4$/PPA2/Li batteries under 40 °C.

batteries with PPA2 was measured in Fig. 4b at 0.1 C under 40 °C. The initial discharge specific capacity of $LiFePO_4$/PPA2(*in-situ*)/Li battery is 146.5 mAh/g, the initial cycle coulomb efficiency is 97.87% and the over-potential between stable charge/discharge potentials is only about 0.14 V, indicating a small resistance of the all-solid-state battery made by *in-situ* method. In 20 cycles, the battery still presents a very flat voltage platform and a relatively low over-potential in the charge/discharge processes. In corresponding, the initial discharge specific capacity of the $LiFePO_4$/PPA2(*ex-situ*)/Li battery is 144.1 mAh/g, over-potential is ~0.2 V in the 1st cycle and increases to ~0.32 V in 20 cycles. Fig. 4c exhibits the cycle performance of $LiFePO_4$/PPA2(*in-situ*)/Li at 0.1 C under 40 °C. The discharge specific capacity of the battery still retains 119.7 mAh/g in 100 cycles, 81.4% of the initial capacity, and the $LiFePO_4$/PPA2(*ex-situ*)/Li battery capacity falls to 90.9 mAh/g in 45 cycles (Fig. S8 in Supporting information). The cyclic performance of the battery basing pure-PEO is also shown in Fig. S9 (Supporting information) which exhibits an initial discharge specific capacity of 125.3 mAh/g and only 71.5 mAh/g in 35 cycles at 0.1 C under 40 °C. These results further prove the better electrochemical stability of the SPE *in-situ* prepared than that of the sample *ex-situ* prepared. The battery constituted by *in-situ* PPA2 presents much smaller polarization potential and better cycle stability than the *ex-situ* one. These should be related to the better interface contact between *in-situ* PPA2 and porous cathode as shown in Fig. 3. The excellent physical contact between the SPE and cathode particles makes the lower interface impedance and denser electrochemically stable component (amide) distributing on cathode surface than those of the *ex-situ* one. Fig. 4d shows rate performance of $LiFePO_4$/PPA2(*in-situ*)/Li battery from 0.1 C to 0.5 C under 40 °C. The discharge capacity of this battery is ~145 mAh/g at 0.1 C, and ~84 mAh/g at 0.5 C. When the rate returns to 0.1 C, most of the discharge capacity is recovered.

Moreover, the SPE PPA2 has been further modified for operating on high potential cathode such as $LiNi_{1/3}Co_{1/3}Mn_{1/3}O_2$. With the addition of 3 wt% LiBOB, the sample PPA2–3%LiBOB shows the better ionic conductivities of 5.99×10^{-5} S/cm at 40 °C and 2.06×10^{-4} S/cm at 60 °C. Then $LiNi_{1/3}Co_{1/3}Mn_{1/3}O_2$/PPA2–3%LiBOB(*in-situ*)/Li battery was assembled and tested (Fig. S10 in Supporting information). The battery shows a reversible discharge specific capacity of 157.9 mAh/g and remains 88.3% in 50 cycles under 0.1 C at 60 °C. With the same electrolyte, the $LiFePO_4$ cathode also shows an initial discharge specific capacity of 165.5 mAh/g and remains 85.3% in 100 cycles at 60 °C, 0.1 C (Fig. S11 in Supporting information). Thus, it is evident that the amide-based composite polymer electrolyte prepared by *in-situ* polymerization can reveal the excellent electrochemical performance and match the needs of cathodes and Li anode for all-solid-state batteries. Beside the good interface contact between PPA2 and electrodes, these also should be attributed to the good electrochemical and thermodynamics stabilities of amide on both of Li and cathodes, which make the thin interface layers and inhibit the blocking and lengthening of the Li ion transmission path from SPE to electrode surfaces.

In summary, a composite polymer electrolyte with the amide-based polymer matrix is prepared successfully by *in-situ* thermal polymerization. The SPE exhibits the excellent capacity of suppressing lithium dendrite growth and makes the Li/PPA2/Li cell work stably for 500 h. PPA2 also presents the favourable interface compatibility between electrolyte and cathode, the good electrochemical stable voltage of 4.7 V *vs.* Li^+/Li, and a remarkable ionic conductivity of 4.25×10^{-5} at 40 °C. However, the electrochemical properties of SPEs are determined by many factors, such as thickness, morphology, which are mainly depends on the detailed technological parameters in battery production process [65]. In another hand, compared with the typical works reported recently as shown in Table S3 (Supporting information) [66–70], the composited polymer electrolyte shown in this work makes $LiFePO_4$ battery deliver 146.5 mAh/g at 0.1 C and remains 119.7 mAh/g in 100 cycles at near-room temperature, similar to the reported PEO-based SPEs and presents an alternative plan for commercial all-solid-state batteries. Moreover, the SPE prepared in this work exhibits excellent extensibility for the utilization of high potential cathode such as $LiCoO_2$ in all-solid-state batteries, meaning the wider application scope of the SPE design strategy our proposed. All these results indicate the potential value of PA-based composite polymer electrolyte in practical application of all-solid-state lithium batteries, and the comprehensive designing strategy can provide the inspiration in designing other high-performance SPEs.

Declaration of competing interest

The authors declare that they have no known competing financial interests or personal relationships that could have appeared to influence the work reported in this paper.

Acknowledgments

This work was supported by the National Natural Science Foundation of China (No. 22075172), Science and Technology Commission of Shanghai Municipality (No. 18010500300) and Ningbo Natural Science Foundation (No. 2019A610015).

References

[1] D. Lin, Y. Liu, Y. Cui, Nat. Nanotechnol. 12 (2017) 194–206.
[2] C. Sun, J. Liu, Y. Gong, D.P. Wilkinson, J. Zhang, Nano Energy 33 (2017) 363–386.
[3] X.B. Cheng, R. Zhang, C.Z. Zhao, Q. Zhang, Chem. Rev. 117 (2017) 10403–10473.
[4] M. Keller, A. Varzi, S. Passerini, J. Power Sources 392 (2018) 206–225.
[5] M. Dirican, C. Yan, P. Zhu, X. Zhang, Mater. Sci. Engin. R Rep. 136 (2019) 27–46.
[6] M.J. Zachman, Z. Tu, S. Choudhury, L.A. Archer, L.F. Kourkoutis, Nature 560 (2018) 345–349.
[7] P. Han, G. Xu, X. Han, et al., Adv. Energy Mater. 8 (2018) 1801243.
[8] A. Manthiram, X. Yu, S. Wang, Nat. Rev. Mater. 2 (2017) 16103.
[9] J.B. Goodenough, K.S. Park, J. Am. Chem. Soc. 135 (2013) 1167–1176.
[10] X.B. Cheng, T.Z. Hou, R. Zhang, et al., Adv. Mater. 28 (2016) 2888–2895.
[11] N.W. Li, Y.X. Yin, C.P. Yang, Y.G. Guo, Adv. Mater. 28 (2016) 1853–1858.
[12] C.A. Geiger, E. Alekseev, B. Lazic, et al., Inorg. Chem. 50 (2011) 1089–1097.
[13] H. Morimoto, H. Awano, J. Terashima, et al., J. Power Sources 240 (2013) 636–643.
[14] T. Ohtomo, A. Hayashi, M. Tatsumisago, et al., J. Power Sources 233 (2013) 231–235.
[15] F. Mizuno, A. Hayashi, K. Tadanaga, M. Tatsumisago, Adv. Mater. 17 (2005) 918–921.
[16] J.H. Wu, L. Shen, Z.H. Zhang, et al., Electrochem. Energ. Rev. 4 (2020) 101–135.
[17] S. Ujiie, T. Inagaki, A. Hayashi, M. Tatsumisago, Solid State Ionics 263 (2014) 57–61.
[18] T. Ohtomo, A. Hayashi, M. Tatsumisago, K. Kawamoto, J. Mater. Sci. 48 (2013) 4137–4142.

[19] R. Komiya, A. Hayashi, Hi. Morimoto, M. Tatsumisago, T. Minami, Solid State Ionics 140 (2001) 83–87.
[20] T. Dong, J. Zhang, G. Xu, et al., Energy Environ. Sci. 11 (2018) 1197–1203.
[21] W. Zhou, Y. Zhu, N. Grundish, et al., Nano Energy 53 (2018) 926–931.
[22] X. Chen, W. He, L.X. Ding, S. Wang, H. Wang, Energy Environ. Sci. 12 (2019) 938–944.
[23] Q. Guo, Y. Han, H. Wang, et al., Electrochim. Acta 296 (2019) 693–700.
[24] Y.-X. Gong, J.J. Wang, Rare Met 39 (2020) 743–744.
[25] X. Zhang, S. Wang, C. Xue, et al., Adv. Mater. 31 (2019) 1806082.
[26] W. Jia, Z. Li, Z. Wu, et al., Solid State Ionics 315 (2018) 7–13.
[27] S. Rajendran, M. Sivakumar, R. Subadevi, Solid State Ionics 167 (2004) 335–339.
[28] E. Quartarone, P. Mustarelli, Chem. Soc. Rev. 40 (2011) 2525–2540.
[29] L. Long, S. Wang, M. Xiao, Y. Meng, J. Mater. Chem. A 4 (2016) 10038–10069.
[30] Q. Liu, Z. Geng, C. Han, et al., J. Power Sources 389 (2018) 120–134.
[31] F. Wu, N. Zhu, Y. Bai, et al., ACS Appl. Mater. Interfaces 8 (2016) 21381–21386.
[32] J. Zhang, J. Zhao, L. Yue, et al., Adv. Energy Mater. 5 (2015) 1501082.
[33] J. Chai, Z. Liu, J. Zhang, et al., ACS Appl. Mater. Interfaces 9 (2017) 17897–17905.
[34] P. Wright, Electrochim. Acta 43 (1998) 1137–1143.
[35] D.S. Decker, D. Teeters, Int. J. Hydrogen Energy 39 (2014) 3025–3035.
[36] J. Przyluski, W. Wieczorek, Solid State Ionics 36 (1989) 165–169.
[37] C. Sun, J. Dong, X. Lu, et al., Adv. Funct. Mater. 31 (2021) 2100594.
[38] Y. Li, Z. Sun, D. Liu, et al., Energy Environ. Mater. 4 (2021) 434–443.
[39] Y. Li, L. Zhang, Z. Sun, et al., J. Mater. Chem. A 8 (2020) 9579–9589.
[40] O. Sheng, J. Zheng, Z. Ju, et al., Adv. Mater. 32 (2020) 2000223.
[41] C. Fu, C. Battaglia, ACS Appl. Mater. Interfaces 12 (2020) 41620–41626.
[42] F. Croce, L. Settimi, B. Scrosati, D. Zane, J. New. Mat. Electrochem. Syst. 9 (2006) 3–9.
[43] L. Fan, Solid State Ionics 164 (2003) 81–86.
[44] W. Liu, N. Liu, J. Sun, et al., Nano Lett 15 (2015) 2740–2745.
[45] H. Ling, L. Shen, Y. Huang, et al., ACS Appl. Mater. Interfaces 12 (2020) 56995–57002.
[46] D. Zhang, X. Xu, X. Huang, et al., J. Mater. Chem. A 8 (2020) 18043–18054.
[47] Z. Yao, K. Zhu, X. Li, et al., ACS Appl. Mater. Interfaces 13 (2021) 11958–11967.
[48] M.L. Verma, H.D. Sahu, Ionics (Kiel) 23 (2017) 2339–2350.
[49] X.X. Zeng, Y.X. Yin, N.W. Li, et al., J. Am. Chem. Soc. 138 (2016) 15825–15828.
[50] J. Zhang, J. Yang, T. Dong, et al., Small 14 (2018) 1800821.
[51] B. Zhang, Y. Zhang, N. Zhang, et al., J. Power Sources 428 (2019) 93–104.
[52] X. Yu, L. Xue, J.B. Goodenough, A. Manthiram, Adv. Funct. Mater. 31 (2020) 2002144.
[53] J. Hu, P. He, B. Zhang, B. Wang, L.Z. Fan, Energy Storage Mater. 26 (2020) 283–289.
[54] L. Liu, J. Mo, J. Li, et al., J. Energy Chem. 48 (2020) 334–343.
[55] S. Huang, Z. Cui, L. Qiao, et al., Electrochim. Acta 299 (2019) 820–827.
[56] H.L. Lyu, C.J. Jafta, I. Popovs, et al., J. Mater. Chem. A 7 (2019) 17888–17895.
[57] Q. Wang, D. Sun, X. Zhou, et al., ACS Appl. Mater. Interfaces 12 (2020) 25826–25831.
[58] Y. Liu, Y. Qin, Z. Peng, et al., J. Mater. Chem. A 3 (2015) 8246–8249.
[59] Y. Liu, D. Sun, J. Zhou, et al., ACS Appl. Mater. Interfaces 10 (2018) 11305–11310.
[60] J. Bao, G. Shi, C. Tao, et al., J. Power Sources 389 (2018) 84–92.
[61] C. Li, Y. Huang, X. Feng, Z. Zhang, P. Liu, J. Membrane Sci. 587 (2019) 1171 79.
[62] A.R. Polu, H.W. Rhee, J. Indust. Eng. Chem. 31 (2015) 323–329.
[63] Z. Qiu, C. Liu, J. Xin, et al., ACS Sustain. Chem. Engin. 7 (2019) 9875–9880.
[64] J. Liang, Q. Sun, Y. Zhao, et al., J. Mater. Chem. A 6 (2018) 23712–23719.
[65] L. Han, C.T. Hsieh, B.C. Mallick, et al., Nanoscale Adv. 3 (2021) 2728–2740.
[66] X.W. Huang, S.Y. Liao, Y.D. Liu, et al., Electrochim. Acta 389 (2021) 138747.
[67] X. Zheng, K. Liu, T. Yang, et al., J. Alloys Compd. 877 (2021) 160307.
[68] H. Erabhoina, D. Rosenbach, J. Mohanraj, et al., Electrochim. Acta 387 (2021) 138455.
[69] J. Tan, X. Ao, H. Zhuo, et al., Chem. Engin. J. 420 (2021) 127623.
[70] R. Li, H. Hua, Y. Zeng, et al., J. Energy Chem. 64 (2022) 395–403.